Supplementary Information (SI) for Inorganic Chemistry Frontiers.

Supporting Information

Tunable Collinear-to-Canted Antiferromagnetic Transition in Co(II)-Based MOFs through Structural Control of Linker Length

Sunghyun Kim[a,†], *Gyuwon Lee*[b,†], *Sarah S. Park*[b]*, *Kwanghyo Son*[c]*, *Hyunchul Oh*[a,d] *

[a] *Department of Chemistry, Ulsan National Institute of Science and Technology (UNIST), Ulsan 44919, Republic of Korea*

[b] *Department of Chemistry, Pohang University of Science and Technology (POSTECH), Pohang 37673, Republic of Korea*

[c] *Department of Physics Education, Kongju National University, Gongju 32588, Republic of Korea*

[d] *Graduate School of Carbon Neutrality, Ulsan National Institute of Science and Technology, 44919 Ulsan, Republic of Korea*

† Equally Contributed.

**Corresponding authors e-mail addresses*: sarahpark@postech.ac.kr, kson@kongju.ac.kr and hcoh@unist.ac.kr

Table of Contents **_Page_**

1. Synthesis of MOFs

The samples were synthesized according to the reported synthetic method. [1, 2] Co_2Cl_2(BBTA) samples were prepared by dissolving H_2BBTA in DMF, followed by mixing with a solution of $CoCl_2 \cdot 6H_2O$ in ethanol and hydrochloric acid. The resulting mixture was heated at 338 K for 10 days. The obtained solids were filtered and washed several times with DMF and methanol, followed by solvent exchange using Soxhlet extraction with methanol. Subsequently, the samples were activated at 373 K under dynamic vacuum for 24 hours. Co_2Cl_2(BTDD) samples were synthesized using the same procedure, with H_2BTDD replacing H_2BBTA as the organic linker. The obtained samples were also subjected to Soxhlet extraction with methanol, followed by activation at 373 K under dynamic vacuum for 24 hours.

2. Physical characterizations

Powder X-ray diffraction (PXRD)

X-ray diffraction (XRD) measurements were carried out using a Rigaku MiniFlex 600 diffractometer equipped with a Cu Kα radiation source ($\lambda = 1.5406$ Å) and a Cu Kβ filter. The X-ray source was operated at an accelerating voltage of 40 kV and a current of 15 mA.

3. Magnetic measurements

The magnetic properties were characterized using a Physical Property Measurement System Vibrating Sample Magnetometer (PPMS VSM) by Quantum Design. The temperature dependence of the magnetic susceptibility was measured in the temperature range of 2 K to 300 K under an applied magnetic field of 1000 Oe, using both zero-field-cooled (ZFC) and field-cooled (FC) protocols. The field dependence of the magnetization was measured for Co_2Cl_2(BBTA) in the temperature range of 2 K to 5 K, and for Co_2Cl_2(BTDD) in the range of 2 K to 8 K, with the applied magnetic field varying from 0 to 7 T. All data were corrected for diamagnetic background signals from the capsule and ligand.

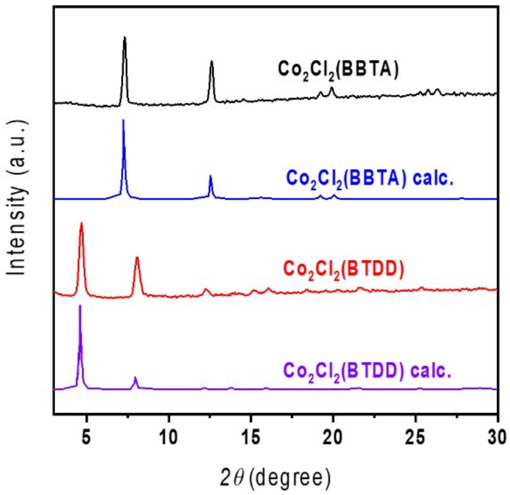

Figure S1. PXRD pattern of Co_2Cl_2(BBTA) and Co_2Cl_2(BTDD).

Powder X-ray diffraction (PXRD) measurements were performed to confirm the crystallinity and phase purity of Co_2Cl_2(BBTA) and Co_2Cl_2(BTDD). As shown in Figure S1, the experimental patterns for both samples are in good agreement with the simulated patterns based on single-crystal data, indicating phase-pure products.

Co_2Cl_2(BBTA) crystallizes in the monoclinic space group *C2/m*, with unit cell parameters a = 19.23 Å, b = 19.23 Å, c = 6.73 Å, $\alpha = \gamma = 90°$, and $\beta = 120°$. In contrast, Co_2Cl_2(BTDD) adopts a trigonal structure in space group $R{-}3m$, with unit cell parameters $a = b$ = 38.66 Å, c = 8.56 Å, $\alpha = \beta = 90°$, $\gamma = 120°$. The PXRD patterns clearly differentiate the two compounds based on distinct peak positions and intensities, consistent with their differing crystallographic symmetries and linker lengths. These results provide direct structural evidence supporting the divergence in their interchain distances.

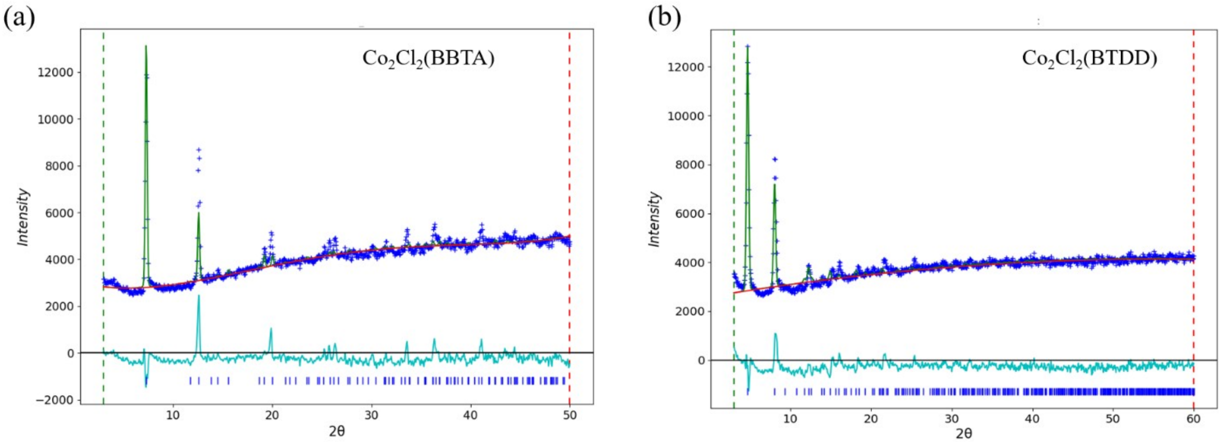

Figure S2. Rietveld refinement plot of (a) Co_2Cl_2(BBTA) and (b) Co_2Cl_2(BTDD) PXRD data. The blue crosses(+) represent the experimental data, the solid red line is the calculated profile, the green line is the background and the line at the bottom represents the difference curve.

Co_2Cl_2(BBTA) and Co_2Cl_2(BTDD) PXRD data were collected to confirm the phase purity and validity of the crystal structure models used in the magnetic analysis. The analysis was performed using the Rietveld refinement against the experimental PXRD patterns (Figure S2).

Rietveld refinement Results: The refinement confirmed the intended structural models and high phase homogeneity. The final refinement achieved good weighted profile R values (R_w) of 5.541% for BBTA and 4.698% for BTDD. The relatively high GOF values (GOF = 3.55 for BBTA and GOF = 2.92 for BTDD) are thought to be attributed to the complex structure of the metal-organic framework. The low R_w values and the visual alignment of the calculated profile and the observed pattern demonstrate that the structural models are accurate and adequately confirmed.

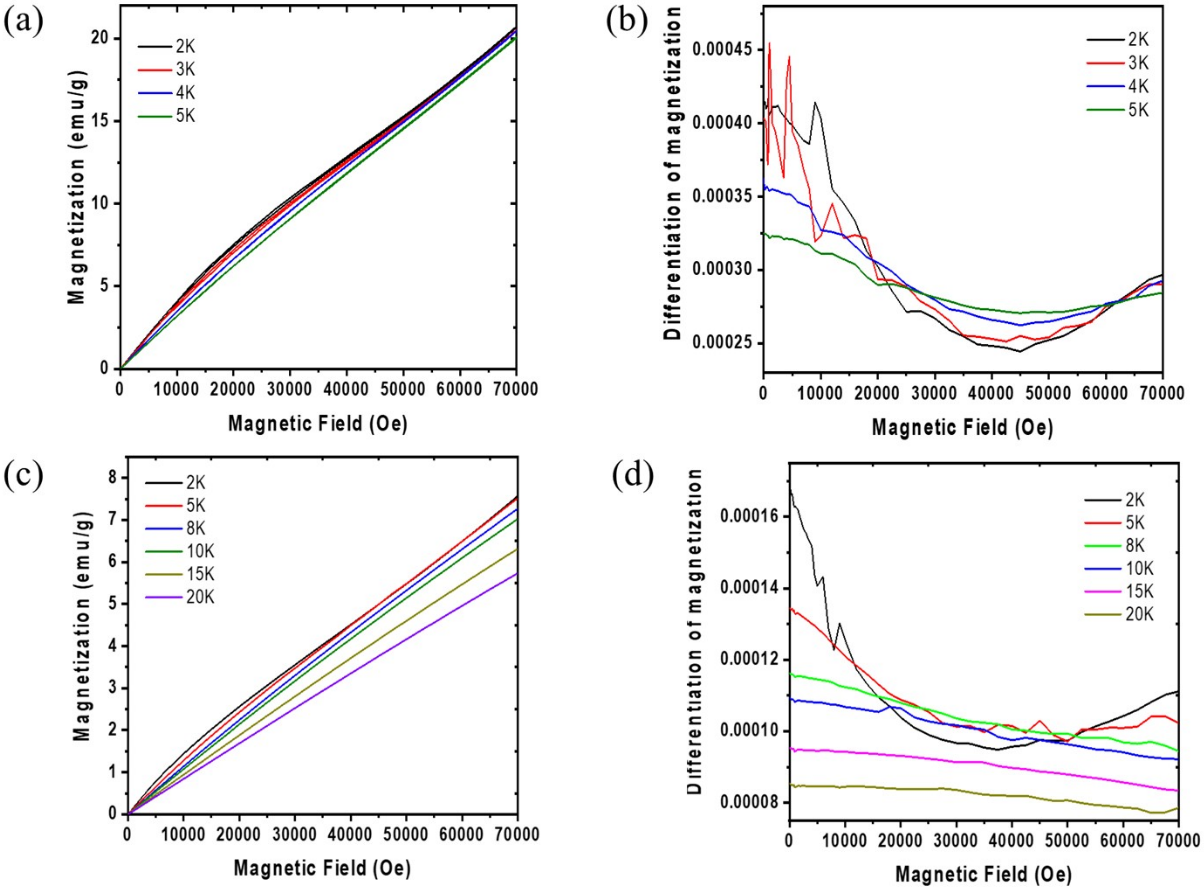

Figure S3. Temperature change of the field-dependent magnetization. (a) M-H curves for Co_2Cl_2(BBTA) at T = 2, 3, 4, and 5 K. (b) Corresponding dM/dH plots for BBTA. (c) M-H curves for Co_2Cl_2(BTDD) at T = 2, 5, 8, 10, 15, and 20 K. (d) Corresponding dM/dH plots for BTDD.

Figure S2 shows the temperature evolution of the field-dependent magnetization for both compounds. For Co_2Cl_2(BBTA) (Figure S2(a)), the M-H curve at 2 K exhibits a clear nonlinear behavior and weak hysteresis. This nonlinear component is thermally suppressed and the curve becomes progressively more linear as the temperature is increased to 5 K. This trend is also evident in the corresponding derivative plots (Figure S2(b)). In contrast, Co_2Cl_2(BTDD) (Figure S2(c)) displays a consistently linear M-H response across the entire measured temperature range (2 K to 20 K), indicating a stable collinear antiferromagnetic state. The corresponding derivative plots (Figure S2(d)) are nearly constant, confirming the absence of any significant nonlinear magnetic component. These observations provide further support for the conclusion that the magnetic ground state is critically dependent on the interchain distance.

The table below summarizes all variables employed in the dual canted antiferromagnetic chain model (Equation 4 in MS), describing both intra- and interchain magnetic contributions, as well as spin canting effects and empirical correction terms used in fitting χT vs T data.

Table S1. Description of fitting parameters used in the dual canted antiferromagnetic chain model

Parameter	Symbol	Unit	Physical Meaning
Intrachain exchange interaction constant	J	K	Strength of AFM interaction between neighboring spins within the chain
Interchain exchange interaction constant	J'	K	Exchange strength between adjacent chains (included via λ)
Interchain coupling parameter	λ	$\mathrm{mol \cdot Oe \cdot emu^{-1}}$	Mean-field approximation parameter reflecting interchain interactions
Intrachain magnetic contribution constant	C_{intra}	$\mathrm{emu \cdot K \cdot mol^{-1} \cdot Oe^{-1}}$	Scaling factor for the magnetic contribution from intrachain interactions
Spin canting contribution constant	C_{cant}	$\mathrm{emu \cdot K \cdot mol^{-1} \cdot Oe^{-1}}$	Scaling factor for the weak ferromagnetic component due to spin canting
Spin canting angle	ϕ	rad (or °)	Deviation angle between antiparallel spins in a canted AFM configuration
Spin canting Weiss temperature	θ_{cant}	K	Effective Weiss temperature associated with the spin canting contribution
Proportional constant	a	–	Dimensionless normalization or scaling factor within χ_{intra}
Number of nearest-neighbor chains	z	–	Coordination number of spin chains considered in the interchain interaction
Residual slope constant	D	$\mathrm{emu \cdot K \cdot mol^{-1} \cdot Oe^{-1}}$	Empirical slope term accounting for background or non-ideal contributions
Residual offset temperature	θ_{res}	K	Constant offset temperature used to improve χT fitting accuracy

[Reference]

1. Rieth, A. J., et al., *Tunable Metal–Organic Frameworks Enable High-Efficiency Cascaded Adsorption Heat Pumps.* Journal of the American Chemical Society, 2018. **140**(50): p. 17591-17596.

2. Rieth, A. J., et al., *High and Reversible Ammonia Uptake in Mesoporous Azolate Metal–Organic Frameworks with Open Mn, Co, and Ni Sites*. Journal of the American Chemical Society, 2016. **138**(30): p. 9401-9404.